This article has been accepted for publication in IEEE/OSA Journal of Lightwave Technology. This is the author's version which has not been fully edited and content may change prior to final publication. Citation information: DOI 10.1109/JLT.2022.3228506

Fiber Bragg Grating Spectra in Graded-index Multimode Optical Fibers

Ying-Gang Nan, Junjun Pan, Fu Liu, Xuehao Hu, and Patrice Mégret

***Abstract*—In this paper, we describe a simulation method to analyze the spectral properties of fiber Bragg gratings written in silica-based multimode graded-index fiber, and compare the simulation results with experimental spectra measured in Bragg gratings made in a commercially available graded-index silica fiber. The simulation provides the locations of the resonance wavelengths and uses the coupled-mode theory and the modal field equations to find the detail of the reflection and transmission spectra. A good agreement between the simulation and the experimental results is found.**

***Index Terms*—Fiber Bragg gratings (FBGs), multimode fiber (MMF), graded-index, coupling coefficient, FBG spectra.**

I. Introduction

FIBER Bragg gratings in multimode optical fibers (MMF) have attracted more and more attention due to their excellent properties useful for many applications [1]–[6]. For example, (1) mode group multiplexing can be used to multiply the capacity of high-speed data transmission in [1] for optical communications, and (2) a gold-coated MMF Tilted Fiber Bragg grating (TFBG) depicts a refractometer with a sensitivity of 134.89 nm/RIU, an enhancement of approximately 22 % compared to TFBG of single-mode fiber for sensing in [2]. The spectral characteristics of FBGs have been investigated by many researchers and interesting results are disclosed in articles [7]–[12]. In [7], many types of gratings were investigated including uniform, apodized, chirped, discrete phase-shifted, and superstructure gratings; short-period and long-period gratings; symmetric and tilted gratings; cladding-mode and radiation-mode coupling gratings. However, for the uniform fiber Bragg grating computation, only the singlemode fiber was analyzed [7]. For FBGs in multimode fibers, [11] and [8] report the characteristics of the experimental spectra and the number of the principal modes, respectively. Computation of the FBG spectra are discussed in [9] and [10], where this latter presents a numerical method based on the fourth-order Runge-Kutta formula to solve the coupled-mode equations between the LP_{01} and LP_{11} modes, without any experimental verification. The authors in [9] report a method describing mode coupling effects in MMF by using the transfer matrix formalism. This method results in a concise equation to compute the FBG spectra in multimode graded-index fiber, and two experimental systems are used to measure the reflection spectra.

Although these simulation methods are helpful to understand the properties of the FBG spectra in multimode grade-index fiber, most of them are limited to the coupling between a few number of modes. In this work, we use the coupled-mode equations to compute the coupling between much more modes of the optical fiber. Moreover, the relations between the spectra profile and the FBG structures (i.e., symmetric and asymmetric) are investigated in this work. In particular, we compute the interactions between all the mode groups [8] and the cross-mode groups [3] that can propagate into the fiber. This finally gives the theoretical reflection spectra and transmission spectra, that can be compared with the experimental ones.

The paper is organized as follows. In the section II, we detail the simulation carried out to compute the grating spectra, whereas experimental results are presented in section III and IV.

II. Theory and Simulation

To compute the FBG spectra in a multimode graded-index fiber, two theoretical tools are needed (1) the propagation equations in a graded-index fiber, and (2) the coupled-mode theory. These two theories are well-known, and can be found in many books like [13]–[16]

Firstly, the resonance wavelengths are calculated among all the mode groups and cross-mode groups. Then, all the coupling coefficients of the mode groups and the cross-mode groups are computed by applying the coupled-mode theory. From the resonance wavelengths and the coupling coefficients, the FBG spectra of the graded-index multimode fiber are simulated when appropriate boundary conditions are specified.

A. Resonance Wavelength calculations

For a parabolic graded-index (GI) multimode fibers (MMF), the refractive index profile is given by

$$n^2(r) = \begin{cases} n_{\mathrm{co}}^2\left(1 - 2\Delta\frac{r^2}{a^2}\right) & 0 \le r \le a, \\ n_{\mathrm{cl}}^2 & r \ge a, \end{cases} \tag{1}$$

where a is the core radius, n_{co} and n_{cl} are the refractive indices at $r = 0$ and $r = a$, respectively, and $\Delta = (n_{\mathrm{co}}^2 - n_{\mathrm{cl}}^2)/2n_{\mathrm{co}}^2$ is the index difference between the core and the cladding. The

This research has been supported by the Fonds de la Recherche Scientifique - FNRS (T.0163.19 "RADPOF"), and the Postdoctoral Researcher grant (C.R.) of Xuehao Hu (FRS-FNRS).(Corresponding authors: Y.-G. Nan)

Y.-G. Nan, X. Hu and P. Mégret are with the Electromagnetism and Telecommunication Department, University of Mons, 31 Boulevard Dolez, Mons, 7000, Belgium(e-mail: yinggang.nan@umons.ac.be; xuehao.hu@umons.ac.be; patrice.megret@umons.ac.be)

J. Pan is with the Department of Mathematics, The University of Hong Kong, Pokfulam, Hong Kong(e-mail: junjpan@hku.hk)

F. Liu is with the Department of Electronics, Carleton University, Ottawa, Ontario K1S 5B6, Canada(e-mail: fuliu0105@gmail.com)

© 2022 IEEE. Personal use is permitted, but republication/redistribution requires IEEE permission. See https://www.ieee.org/publications/rights/index.html for more information.

This article has been accepted for publication in IEEE/OSA Journal of Lightwave Technology. This is the author's version which has not been fully edited and content may change prior to final publication. Citation information: DOI 10.1109/JLT.2022.3228506

estimated number N of modes that can propagate in GI MMF is given by [16]

$$N = \frac{V^2}{4}, \tag{2}$$

where $V = (2\pi a \mathrm{NA})/\lambda$ is the normalized frequency with $\mathrm{NA} = \sqrt{n_{\mathrm{co}}^2 - n_{\mathrm{cl}}^2} = n_{\mathrm{co}}\sqrt{2\Delta}$ the numerical aperture.

In this work, we use a commercially available graded-index MMF (Corning 50/125), with a core diameter, a cladding diameter and a numerical aperture of 50 µm, 125 µm and 0.2, respectively [17]. Using (2), the estimated number N of modes LP_{lv} that can propagate in this fiber is $\mathrm{N} \approx 100$ as $n_{\mathrm{co}} \approx 1.4585$ and $\lambda = 1550\,\mathrm{nm}$. Although there is a significant number of modes LP_{lv} that can propagate, a detailed analysis of the individual modal propagation constants β_{lv} in GI MMF [18], [19] reveals that modes LP_{lv} can be clustered in groups of modes indexed by $m = l + 2v - 1$: each mode within a group has the same propagation constant β_m [13], and this propagation constant significantly changes from mode group to mode group.

There are different methods to analyze the mode propagation in parabolic graded-index multimode fiber, such as infinite medium approximation [19], [20], perturbation approximation [21], variational analysis [22], rigorous scalar wave analysis [23], and staircase approximation [24]. In this work, we use the infinite medium approximation method to analyze the characteristics of the modes propagation in our fiber. Using the expression of the propagation constants in [19], [20], the normalized propagation constant b is expressed as

$$b = 1 - \frac{2m}{\mathrm{V}}, \tag{3}$$

where m is the order of the mode group.

Fig. 1 plots Eq. (3), i.e., b versus the normalized frequency V number, and shows that the number of such mode groups corresponds to the expression derived in [8], [18], [25]

$$M = \sqrt{N} = \frac{V}{2}. \tag{4}$$

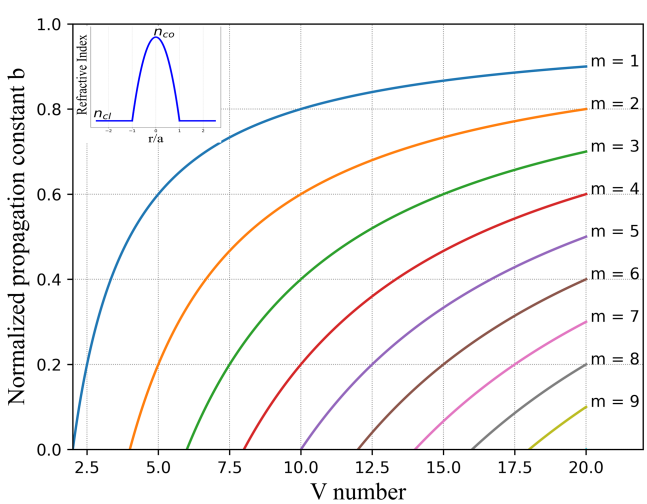

Fig. 1. Plots of V number and normalized propagation constant for a parabolic graded-index fiber, and the refractive index profile (inset).

For the graded-index multimode Corning 50/125 fiber, for $V \approx 20$, the number M of mode groups is $M \approx 10$ which agrees with the results of Fig. 1.

In the following, we will use the subscript m to describe a mode group, and we will consider $m = 1, 2, 3, \ldots, 10$ for the GI Corning 50/125 MMF. The effective refractive index n_m of the mth mode group can be expressed as [3], [8], [13]

$$n_m = n_{\mathrm{co}}\sqrt{1 - 4m\Delta/\mathrm{V}}. \tag{5}$$

Following reference [8], the cross-mode group parameter is used to describe a mode stimulated by the two neighboring mode groups m and $m{+}1$ in a fiber Bragg structure. According to the Bragg wavelength equation $\lambda_{\mathrm{Bragg}} = 2n_{\mathrm{eff}}\Lambda$, the resonance wavelengths of the mth mode group and m^{th} cross-mode group are given by

$$\lambda_m = 2n_m\Lambda, \tag{6a}$$

$$\lambda_m^{\mathrm{cross}} = (n_m + n_{m+1})\Lambda. \tag{6b}$$

Using (5), (6a) and (6b), the wavelength spacing between two adjacent mode group reflection peaks is equal to [8]

$$\Delta\lambda = \frac{\lambda_0^2 \mathrm{NA}}{2\pi a n_{\mathrm{co}}^2}. \tag{7}$$

Table I gives the computed resonance wavelengths of the mth mode group and m^{th} cross-mode group for a grating period of $\Lambda = 530\,\mathrm{nm}$ that corresponds to the one made experimentally in section III.

TABLE I
DISTRIBUTION OF COMPUTED BRAGG RESONANCE WAVELENGTHS IN CORNING 50/125 GI MMF FIBER

m	n_m	λ_m (nm)	$\lambda_m^{\mathrm{cross}}$ (nm)
1	1.4601	1547.66	1546.92
2	1.4587	1546.19	1545.45
3	1.4573	1544.71	1543.97
4	1.4559	1543.23	1542.49
5	1.4545	1541.75	1541.00
6	1.4531	1540.26	1539.52
7	1.4517	1538.78	1538.04
8	1.4503	1537.29	1536.55
9	1.4489	1535.81	1535.06
10	1.4475	1534.32	

B. Coupling Theory

The fiber Bragg grating (FBG) is a periodic variation of the refractive index of the core, which generates a wavelength specific dielectric mirror. It reflects particular wavelengths of the light and transmits all others. Fig. 2 shows the schematic of an FBG in the fiber, and illustrates the symmetry of the grating structure relative to the fiber axis.

Currently, there are many different methods to compute the FBG spectra in the optical fiber such as coupling equation method [7], transverse matrix method [26], and Monte Carlo method [27]. Here we use the coupled-mode equations as a straightforward and accurate method to get the FBG spectra in the MMF. To simplify, two approximations are nevertheless made:

© 2022 IEEE. Personal use is permitted, but republication/redistribution requires IEEE permission. See https://www.ieee.org/publications/rights/index.html for more information.

This article has been accepted for publication in IEEE/OSA Journal of Lightwave Technology. This is the author's version which has not been fully edited and content may change prior to final publication. Citation information: DOI 10.1109/JLT.2022.3228506

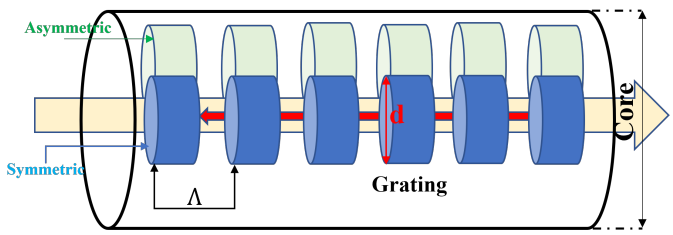

Fig. 2. Schematic of FBG with symmetrical and asymmetrical structures in GI MMF Fiber.

- according to Olshansky's selection rules, the coupling is dominant by transitions between neighboring two mode groups [13], [18], [25];
- "synchronous approximation" [7] and simplified mode differential equation are used [15].

The power differential equations for two counter-propagating mode groups m and l can be found in [10], [28]. Furthermore, for a uniform grating, the coupling coefficient of two mode groups is described by the following equation [7], [13], [29]

$$\kappa_{m,l}(z) = \frac{\upsilon\omega\epsilon_0}{8}\iint_{S_{cos}} \Delta\epsilon(z)\vec{\psi}_m\vec{\psi}_l^* \,\mathrm{d}S\,, \tag{8}$$

where S_{cos} is the cross-section of the grating, ω is the angular frequency, ϵ_0 is dielectric permittivity of the free space, $\Delta\epsilon(z) = 2n\overline{\delta n}(z)$, $\overline{\delta n}(z)$ is the refractive index change in the core, and υ is the fringe visibility. In the particular of the self-coupling, the coefficient $\kappa_{m,m}$ is simply written as κ_m. The most important parameter in (8) is the transverse field profile distribution ($\vec{\psi}_m(r,\varphi)$). Here, we use the weak guiding approximation as a concise and straightforward method to compute the transverse field profile because most practical graded-index MMFs, including the one used in our experiment, are weakly guiding, that is the relative index difference $\Delta \ll 1$ [13]. In this approximation, the modes are assumed to be nearly transverse and have an arbitrary state of polarization [13]. Now, in theory, if we put the field profile equation of mode groups m and $m+1$ into (8), we obtain $\kappa_{m,m+1}$. However, in practice, the grating diameter is usually less than the fiber core diameter, and depending of the setup alignment, two FBG structures are possible, i.e., symmetric and asymmetric as shown in Fig. 2. The cross-section S_{cos} is expressed in polar coordinates as $\int_0^{r^*}\int_0^{\varphi^*} r\mathrm{d}r\mathrm{d}\varphi$, where r^* and φ^* represent the grating radius (0 to $\frac{d}{2}$) and the fiber cross-section angles ($\leq 2\pi$). For centered and symmetrical gratings, $\Delta\epsilon(r,\varphi,z)$ has a cylindrical symmetry around the fiber axis and $\kappa_{m,m+1}$ is zero. For asymmetric gratings, $\Delta\epsilon(r,\varphi,z)$ is no longer centered on the fiber axis, and has no longer a cylindrical symmetry. This impacts all the coupling coefficients, but the effect is much more visible on $\kappa_{m,m+1}$ that is no longer equal to zero.

On the one hand, the radius of the grating ($\frac{d}{2}$ in Fig. 2) influences the values of the self-coupling coefficients κ_m in (8). In this simulation, the refractive index change and the fringe visibility are $\overline{\delta n} = 8.5\times10^{-4}$ and $\upsilon = 0.1$, respectively. Moreover, the cross-section S_{cos} is a circle centered on the fiber axis with $r^* = \frac{d}{2}$ and $\varphi^* = 2\pi$ (symmetrical grating). Figure 3 represents the self-coupling coefficients distribution among different mode groups (first five mode groups) with the increase of the radius of the grating ($\frac{d}{2}$) in the cross section of fiber core. As mode groups are made of a mixture

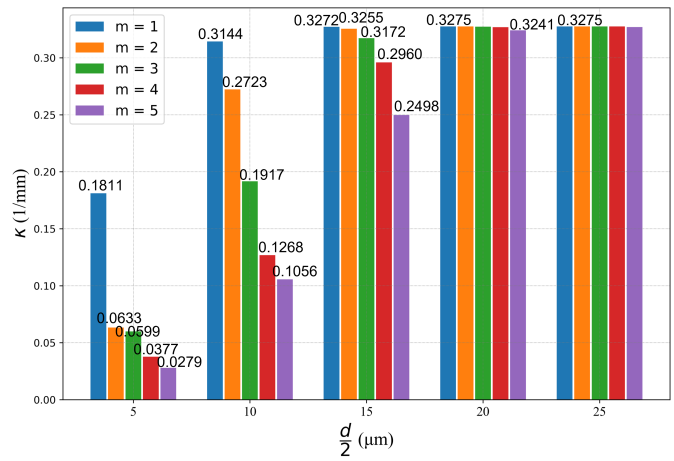

Fig. 3. Distribution of self-coupling coefficients in different mode groups for symmetrical gratings with radius ($\frac{d}{2}$).

of LP modes [13], we computed the coupling coefficients as an average. For example, the third mode group ($m = 3$) is a combination of LP_{21} and LP_{02} [19], so we evaluate κ_3 by $(\kappa_{\mathrm{LP}_{21}} + \kappa_{\mathrm{LP}_{02}})/2$. It is clear in Fig. 3 that the self-coupling coefficient decreases with the increase of the order of the mode group, i.e., $\kappa_{m+1} < \kappa_m$ when $\frac{d}{2} < 20\,\mu\mathrm{m}$. All the mode groups reach the maximal self-coupling coefficient when the grating fully covers the core ($\frac{d}{2} = 25\,\mu\mathrm{m}$). Therefore, for given $\overline{\delta n}$ and υ, the first mode group ($m = 1$) shows a dominant resonance peak reflectivity in the FBG spectra during the inscription, and the maximal reflectivities of the other mode groups depend on the $\frac{d}{2}$.

On the other hand, the FBG position inside the core relative to the fiber axis also influences the amplitude of the coupling coefficients. To see this effect, we assume the grating to be located in a circle of radius $\frac{d}{2} = 4\,\mu\mathrm{m}$, but shifted vertically or horizontally relative to the fiber axis as shown in Fig. 4. The first three coupling coefficients (first mode group κ_1, first

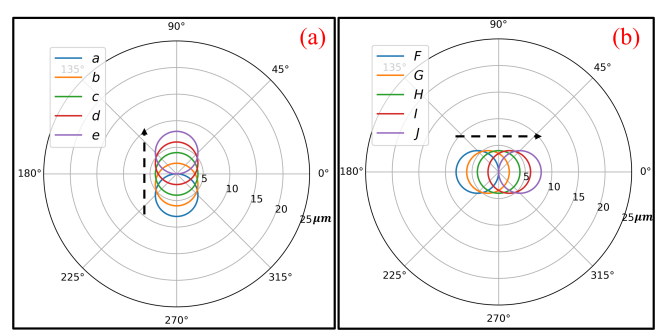

Fig. 4. The evolution of grating locations with two directions: (a) a to e, and (b) F to J in cross section of the fiber core in the polar coordinates.

cross-mode group $\kappa_1^{\mathrm{cross}} = \kappa_{1,2}$, and second mode group κ_2) are computed and monitored with the evolution of the grating locations. Fig. 5 shows that κ_1 has the same behavior

© 2022 IEEE. Personal use is permitted, but republication/redistribution requires IEEE permission. See https://www.ieee.org/publications/rights/index.html for more information.

This article has been accepted for publication in IEEE/OSA Journal of Lightwave Technology. This is the author's version which has not been fully edited and content may change prior to final publication. Citation information: DOI 10.1109/JLT.2022.3228506

vertically and horizontally, whereas it is not the case for the other coefficients. It is due to the angular dependence of the modes: LP_{01} is independent of φ, whereas LP_{11} varies in $\cos(\varphi)$ or $\sin(\varphi)$.

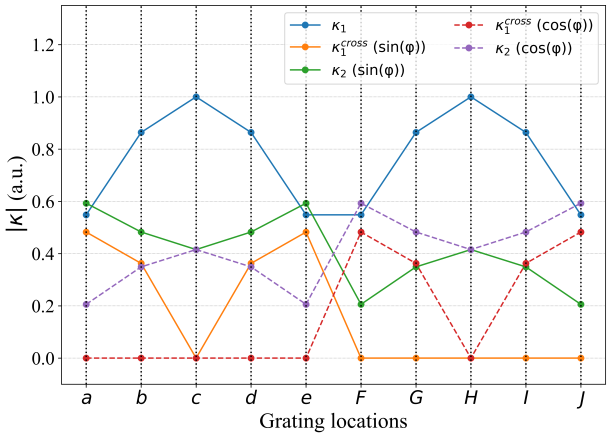

Fig. 5. The evolution of coupling coefficients under different grating locations.

According to the simulation results, the following conclusion are drawn:

- For the first mode group, κ_1 shows the same values for the locations that have the same distance to the core center. In other words, the first mode group coupling coefficient is the independent of the fiber polarization. κ_1 reaches its maximum value when the grating is centered on the fiber axis;
- For the second mode group, κ_2, shows an opposite tendency with the evolution of the grating locations. When LP_{11} is expressed with the $\sin(\varphi)$ function, κ_2 shows a minimum value in location c, and a maximum value in location H. κ_2 shows totally an opposite response to the grating locations evolution when LP_{11} is expressed as $\cos(\varphi)$ function;
- For the first cross-mode group, κ_1^{cross} shows a more complex dependence with the grating locations. When LP_{11} is expressed with the $\sin(\varphi)$ function, κ_1^{cross} equals to 0 in locations F, G, H, I, and J, respectively. However, κ_1^{cross} equals to 0 in locations a, b, c, d, and e when LP_{11} is expressed with the $\cos(\varphi)$ function. It should be noted that κ_1^{cross} always equals to 0 when grating location at the core center, highlighting the fact that the cross-coupling is not possible in symmetric grating.

C. Bragg grating Spectra for symmetric structures

After we get the coupling coefficients of the FBG, the coupled first-order differential equations of two mode groups are analytically solved when appropriate boundary conditions are specified. If R_m and S_m are the amplitudes of the normalized forward and counter propagating mode group m, respectively, the solutions of the coupled equations, with the boundary conditions $R_m(-L/2) = 1$ and $S_m(L/2) = 0$, are given in [29] as

$$R_m(z) = \frac{\alpha_c \cosh(\alpha_c(\frac{L}{2} - z)) + i\tau \sinh(\alpha_c(\frac{L}{2} - z))}{\alpha_c \cosh(\alpha_c L) + i\tau \sinh(\alpha_c L)} e^{i\tau(z+\frac{L}{2})}, \tag{9}$$

$$S_m(z) = \frac{i\kappa_m \sinh(\alpha_c(\frac{L}{2} - z))}{\alpha_c \cosh(\alpha_c L) + i\tau \sinh(\alpha_c L)} e^{-i\tau(z+\frac{L}{2})}. \tag{10}$$

where $\alpha_c = \sqrt{\kappa_m^2 - \tau^2}$ and τ is phase mismatch.

It is worth to note that $R_m(-L/2) = 1$ for any m implicitly means that all the modes carry the same power before entering the grating.

The solutions for the mode group have the same shapes as the solutions for the FBG in singlemode fiber [7]; therefore we get the reflected amplitudes B_m at $z = -L/2$,

$$B_m = \frac{S_m(-L/2)}{R_m(-L/2)}. \tag{11}$$

and from which the corresponding reflectivities are computed by

$$r_m = |B_m|^2. \tag{12}$$

or explicitly

$$r_m = \frac{\sinh^2(|\kappa_m| L\sqrt{1 - |\tau/\kappa_m|^2})}{\cosh^2(|\kappa_m| L\sqrt{1 - |\tau/\kappa_m|^2}) - |\tau/\kappa_m|^2}. \tag{13}$$

In this simulation, if we set the length of the grating, radius of the grating, refractive index change in the core, and the fringe visibility equal to $L = 9\,\text{mm}$, $d = 8\,\mu\text{m}$, $\overline{\delta n} = 8.5 \times 10^{-4}$, and $\upsilon = 0.1$, respectively, we obtain the maximum reflectivity ($\tau = 0$) of each mode group as shown in Fig. 6. For the FBG inscribed in this graded-index

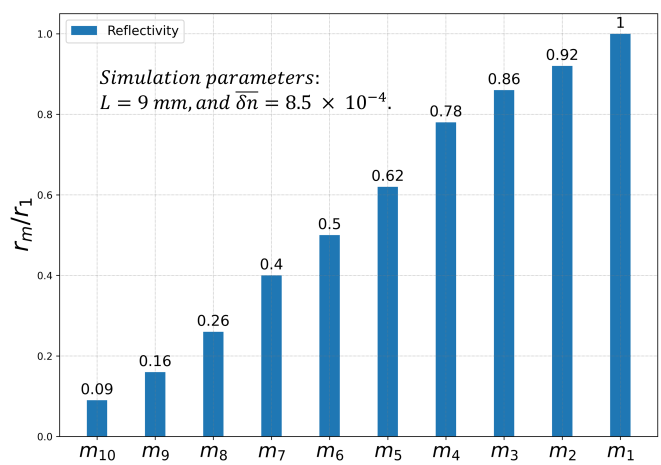

Fig. 6. The change of the reflectivity among different mode groups in grating length $L = 9\,\text{mm}$.

MMF, the first mode group ($m = 1$) shows the maximum reflectivity, and the highest-order mode group ($m = 10$) shows the lowest reflectivity. We also notice that the reflectivities of the higher-order mode groups are significantly decreasing with the increase of the order of the group modes.

In [8], [10], the large resonance wavelengths spacing between two adjacent mode groups is reported, and it also demonstrated by the calculation in Table I. It is clear that

© 2022 IEEE. Personal use is permitted, but republication/redistribution requires IEEE permission. See https://www.ieee.org/publications/rights/index.html for more information.

This article has been accepted for publication in IEEE/OSA Journal of Lightwave Technology. This is the author's version which has not been fully edited and content may change prior to final publication. Citation information: DOI 10.1109/JLT.2022.3228506

the individual mode group resonances do not overlap. As a result, the reflection spectrum of the grating is computed by the sum of the reflection spectra of each mode group.

$$r = \sum_{m=1}^{10} r_m. \tag{14}$$

and the transmission spectrum is

$$t = 1 - r \tag{15}$$

For a 9 mm-long FBG in graded index multimode fiber, the reflection and transmission spectrum are shown in Fig. 7.

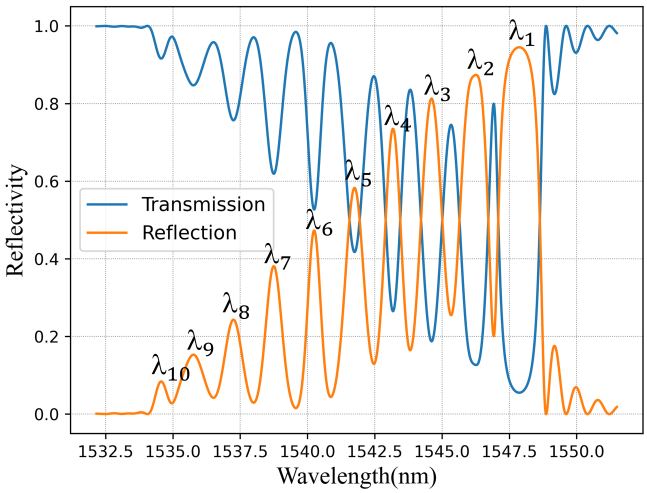

Fig. 7. Reflection and transmission spectra for FBG in graded index fiber with $L = 9\,\mathrm{mm}$.

In the next section, we will design FBG in graded-index fiber and measure the reflection and transmission spectra to assess the above numerical simulations.

III. Experiment

A. Experimental set-up

In this work, we use a commercially available parabolic graded-index MMF (Corning 50/125), with a core diameter, a cladding diameter and a numerical aperture of 50 µm, 125 µm and 0.2, respectively [17]. These fibers are hydrogen-loaded under 205 bar and 55 °C for 60 h to improve the photosensitivity [30].

The FBG fabrication system that we used is a femtosecond pulses laser at 400 nm [3], the period of the phase mask is 1060 nm, and the length of grating is 9 mm. In this work, gratings are inscribed in the same GI multimode fiber with different grating structures (i.e. symmetric and asymmetric) and the same grating length (9 mm). A super-wideband light source (from Amonics) across 1250 nm to 1650 nm, and an optical spectrum analyzer (AQ6370 from YOKOGAWA) with a resolution of 0.02 nm in 600 nm to 1700 nm are connected by the GI MMF (Corning 50/125) to measure the transmission spectra of the FBG during the inscriptions. This OSA has a free space input structure, so that there is no mode filtering when connecting multimode fibers directly to its input [31]. In that way, we avoid any SMF-MMF structure, that will distort the spectrum measurements.

We experimentally notice that the FBG spectra are highly linked to beam focusing locations. Figure 8 represents the schematic of the beam focusing inscription setup. The position

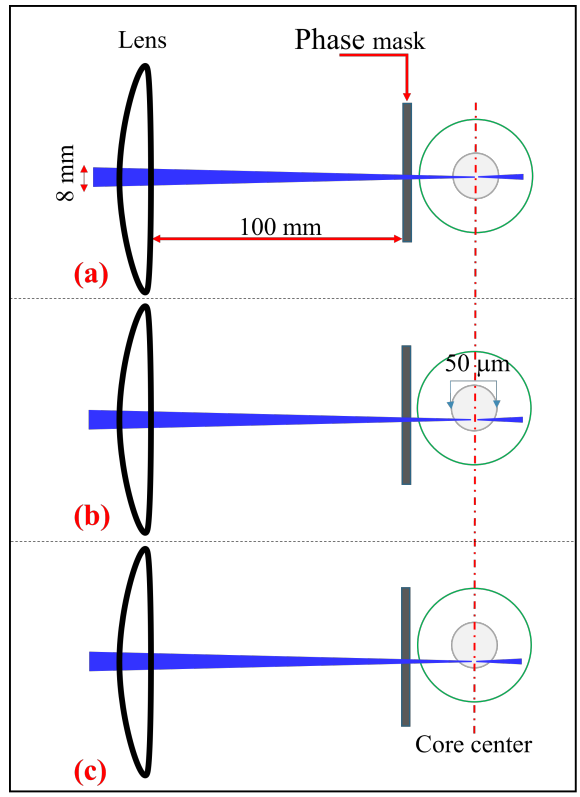

Fig. 8. The schematic of the beam focusing locations: (a) in the fiber core center; (b) small offset of the center; and (c) far away from the center.

of the grating in the core of the fiber is changed by varying the beam focusing point using a micrometer stage (MAX313D from THORLABS company) mounted below the fiber holder. As the beam power has a symmetrical distribution on both sides of the focusing point, symmetrical and asymmetrical grating structures are related to fiber position relative the beam axis, as shown in Fig. 8 (a) and Fig. 8 (b) or (c), respectively.

B. Symmetrical Gratings

Figure 9 represents the evolution of the transmission spectrum during the inscription of a 9 mm-long grating (#1) when the inscription beam is focused in the core center as shown in Fig. 8 (a). The theoretical resonance wavelengths of the mth mode group and m^{th} neighboring cross-mode group are given in Table I and compared with an experimental spectrum of grating #1 in Fig. 9, where the black and red dotted lines represent the resonance wavelength locations of the mode groups and the cross-mode groups, respectively. It should be noted that the cross-mode group peaks did not appear in Fig. 9, which means that the grating is a symmetrical one as expected. The experimental resonance wavelengths have a good agreement with the computed results for the mode group peaks labelled as λ_1, λ_2, λ_3, λ_4, and λ_5. Moreover, the experimental wavelength spacing between two adjacent mode groups is 1.48 nm which is consistent with the computation value of 1.47 nm.

© 2022 IEEE. Personal use is permitted, but republication/redistribution requires IEEE permission. See https://www.ieee.org/publications/rights/index.html for more information.

This article has been accepted for publication in IEEE/OSA Journal of Lightwave Technology. This is the author's version which has not been fully edited and content may change prior to final publication. Citation information: DOI 10.1109/JLT.2022.3228506

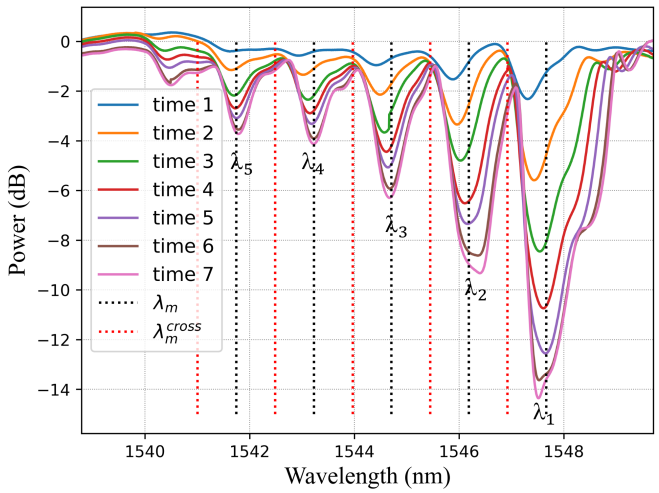

Fig. 9. Experimental FBG spectrum evolution for a 9 mm-long FBG #1 in a parabolic graded-index fiber with a symmetrical grating structure.

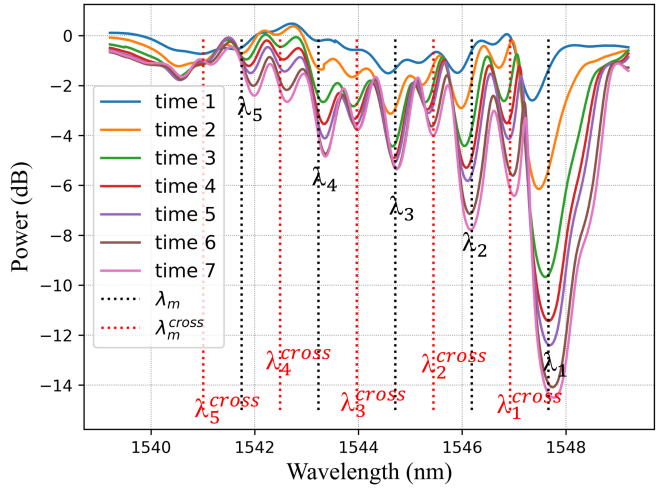

Fig. 11. Experimental FBG spectrum evolution for a 9 mm-long FBG #3 in a parabolic graded-index fiber with an asymmetrical grating structure.

C. Asymmetrical Gratings

Figure 10 shows an FBG spectrum for a 9 mm-long grating (#2) written with a beam slightly off the center as depicted in Fig. 8 (b). It should be noted that now subpeaks appeared

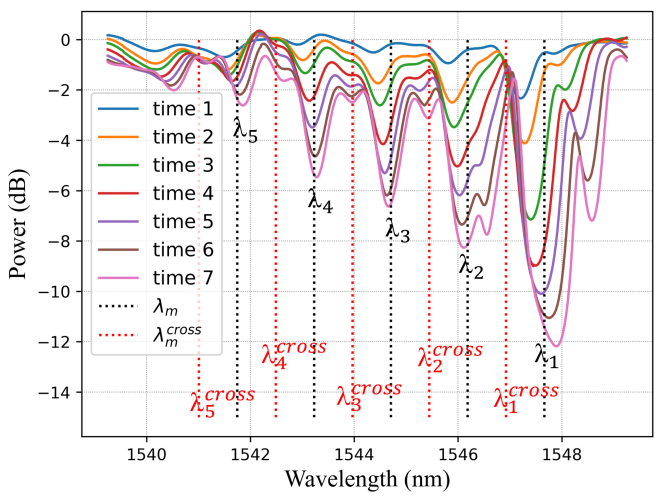

Fig. 10. Experimental FBG spectrum evolution for a 9 mm-long FBG #2 in a parabolic graded-index fiber with an asymmetrical grating structure.

between two adjacent mode group peaks. These subpeaks correspond to the cross-mode groups created by the coupling between two neighbouring mode groups. The experimental resonance wavelengths also have a good agreement with the computed results (see Table I) as shown by the red dotted lines. To further investigate the relation between the beam focusing location and the spectra profile, the focusing point is moved far away from the core center (i.e. Fig. 8 (c)), and Fig. 11 shows the corresponding FBG spectra. It is clearly seen that the cross-mode group peaks are much more stronger in that case. Comparing Figs. 9, 10, and 11, it is clearly seen that: 1) the appearance of the cross-mode groups peaks is highly dependent on the beam focusing positions; 2) the peak power of the higher-order mode groups (λ_2, λ_3, λ_4, and λ_5) relative to the first mode group (λ_1) decreases with the increase of beam focusing offset from the core center; 3) the locations of the resonance wavelength of the mode groups and the cross-mode groups are independent of the locations of the beam focusing point, and are in good agreement with their theoretical values; and 4) the wavelength spacing between two adjacent mode groups is also independent of the locations of the beam focusing point.

IV. Discussion

The spectra evolution versus time of the symmetrical grating (Fig. 9) and the asymmetrical gratings (Figs. 10 and 11) in parabolic graded-index MMF are analyzed to extract the reflectivities of the lower-order mode groups (λ_1 and λ_2). Fig. 12 displays of the reflectivities of grating #1 at times 3 and 5, grating #2 at times 4 and 7, and grating #3 at times 4 and 6, where the times were chosen to have nearly the same reflectivities for the fundamental mode λ_1 in graph (a), and then in graph (b). It is noticed that the reflectivity of the

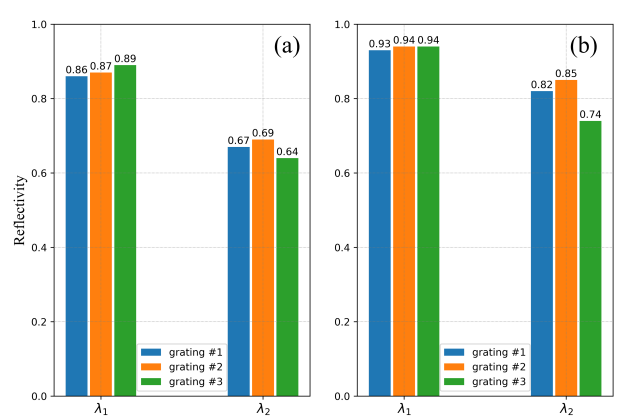

Fig. 12. The reflectivity distribution of two lower-order mode groups for which the fundamental mode peak show approximately the same power.

second mode group (λ_2) has approximately the same value for gratings #1 and #2, but is significantly lower for grating

© 2022 IEEE. Personal use is permitted, but republication/redistribution requires IEEE permission. See https://www.ieee.org/publications/rights/index.html for more information.

This article has been accepted for publication in IEEE/OSA Journal of Lightwave Technology. This is the author's version which has not been fully edited and content may change prior to final publication. Citation information: DOI 10.1109/JLT.2022.3228506

#3. This could correspond to the power transfer to the cross-mode group due to the coupling between the adjacent mode groups, as the strength of the mode coupling is highly linked to the asymmetry of the grating structure.

From the reflectivity r_1 of the first mode group in Fig. 12, the maximum coupling coefficients of gratings #1, #2, and #3 are computed by the relation

$$r_1 = \tanh^2(\kappa_1 L). \tag{16}$$

leading to a coupling coefficient κ_1 approximately equal to $0.1970/\mathrm{mm}$ in Fig. 12 (a), and $0.2525/\mathrm{mm}$ in Fig. 12 (b), respectively. After we got the κ_1 in experimental spectra, using Eq. (8), the refractive index change can be calculated which will be used to compute the values of r_2 to r_{10} in the simulation.

Fig. 13 shows the measured (dotted lines) spectra and the computed (red solid lines) with fitting parameters of $r_1 = 0.86$ and the grating length equal to 9 mm. The full width at half maximum (FWHM) of the measured spectra agrees with the simulation, such as the FWHM of the first mode group. Moreover, it is clear that the FBG experimental reflectivity spectra and and the computed one are in good agreement.

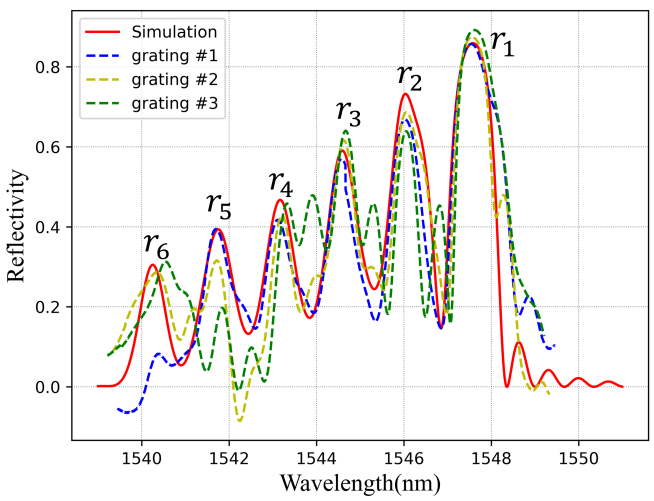

Fig. 13. Comparing between the computed and the experimental spectrums where the $r_1 = 0.86$ in a 9 mm-long FBG.

To explore the reliability of the simulation method and the relation between the FBG spectra and the coupling coefficient (mainly influenced by the refractive index changes of the fiber core), we investigate a 9 mm-long FBG with $|\kappa_1| = 0.2525/\mathrm{mm}$ which corresponds to $r_1 = 0.94$ in Fig. 12 (b). Figure 14 shows the computed and experimentally measured spectra for this 9 mm-long FBG with higher reflectivity in the fundamental mode. It is clear that all the reflectivities of the mode groups are increased with the increase of the refractive index change in the core. It is again found that the experimental spectrum has a good agreement with the simulated one. Moreover, the FWHM of the mode groups is also broader in Fig. 14 than in Fig. 13. For example, in Fig. 13 and Fig. 14, the FWHM of the first mode group are 1.088 nm and 1.568 nm in the computed spectra, respectively.

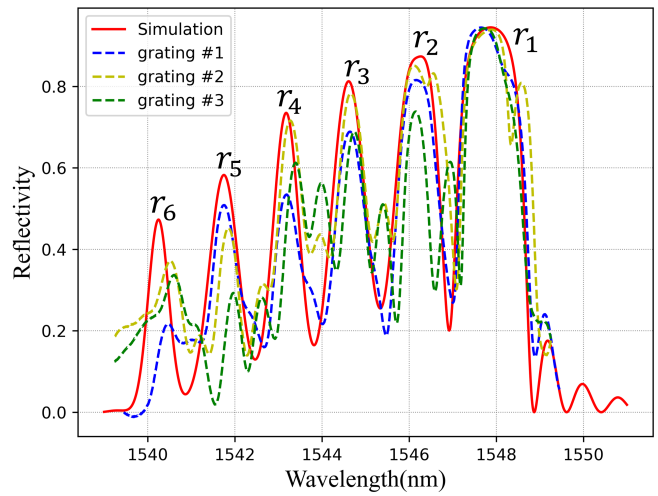

Fig. 14. Comparing between the computed and the experimental spectrums where the $r_1 = 0.94$ in a 9 mm-long FBG.

V. Conclusion

A numerical method has been presented to compute the FBG spectra in the multimode graded-index fiber. In this simulation, we discuss the location of the resonance wavelengths of the FBG. It is shown that the agreement between the experimental spectra and the computed resonance wavelengths is quite good. The reflectivity of all the mode groups are investigated. The reflection and transmission spectra of FBG in Corning 50/125 fiber are obtained using the coupling mode theory.

Among the experimental gratings, two structures are investigated, i.e., the symmetrical and asymmetrical gratings. It is clear that a significant coupling happened between two adjacent mode groups in the FBGs with the asymmetrical structure. This structure will create cross-mode resonance peaks in the spectrum. on the other hand, for a symmetrical grating, only the mode group resonance peaks are present in the spectra. The amplitude of the cross-mode groups is also highly influenced by the power distribution among each mode group resonance peak. A lower amplitude second mode group peak (λ_2) is found in the asymmetrical gratings compared with the symmetrical gratings within the same reflectivity fundamental mode in the experimental spectra. Compared with the FBG simulation spectra, the experimental spectra show a good agreement with the computed ones among the power distribution and resonance wavelengths locations in the mode groups and the cross-mode groups. Thus, it is an excellent candidate to analyze the properties of FBG spectra in graded-index multimode optical fiber.

References

[1] B. Franz and H. Bulow, "Mode group division multiplexing in graded-index multimode fibers," *Bell Labs Technical Journal*, vol. 18, no. 3, pp. 153–172, dec 2013.

[2] M. Lobry, M. Loyez, E. M. Hassan, K. Chah, M. C. DeRosa, E. Goormaghtigh, R. Wattiez, and C. Caucheteur, "Multimodal plasmonic optical fiber grating aptasensor," *Optics Express*, vol. 28, no. 5, p. 7539, feb 2020.

© 2022 IEEE. Personal use is permitted, but republication/redistribution requires IEEE permission. See https://www.ieee.org/publications/rights/index.html for more information.

This article has been accepted for publication in IEEE/OSA Journal of Lightwave Technology. This is the author's version which has not been fully edited and content may change prior to final publication. Citation information: DOI 10.1109/JLT.2022.3228506

[3] Y.-G. Nan, D. Kinet, K. Chah, I. Chapalo, C. Caucheteur, and P. Mégret, "Ultra-fast fiber bragg grating inscription in CYTOP polymer optical fibers using phase mask and 400 nm femtosecond laser," *Optics Express*, vol. 29, no. 16, p. 25824, jul 2021.

[4] C. Broadway, D. Kinet, A. Theodosiou, K. Kalli, A. Gusarov, C. Caucheteur, and P. Mégret, "CYTOP fibre Bragg grating sensors for harsh radiation environments," *Sensors*, vol. 19, no. 13, p. 2853, jun 2019.

[5] D. Vilarinho, A. Theodosiou, M. F. Domingues, P. Antunes, K. Kalli, P. André, and C. A. F. Marques, "Foot plantar pressure monitoring with CYTOP Bragg gratings sensing system," in *Proceedings of the 11th International Joint Conference on Biomedical Engineering Systems and Technologies*, vol. BIODEVICES, 2018, pp. 25–29.

[6] C. Broadway, K. Kalli, A. Theodosiou, M. Zubel, K. Sugden, P. Mégret, and C. Caucheteur, "L-band CYTOP Bragg gratings for ultrasound sensing," in *Micro-Structured and Specialty Optical Fibres V*, vol. 1068109. SPIE, may 2018.

[7] T. Erdogan, "Fiber grating spectra," *Journal of Lightwave Technology*, vol. 15, no. 8, pp. 1277–1294, 1997.

[8] Y. Liu, J. Lit, X. Gu, and L. Wei, "Fiber comb filters based on UV-writing Bragg gratings in graded-index multimode fibers," *Optics Express*, vol. 13, no. 21, p. 8508, 2005.

[9] M. J. Schmid and M. S. Müller, "Measuring Bragg gratings in multimode optical fibers," *Optics Express*, vol. 23, no. 6, p. 8087, mar 2015.

[10] C. Lu and Y. Cui, "Fiber Bragg grating spectra in multimode optical fibers," *Journal of Lightwave Technology*, vol. 24, no. 1, pp. 598–604, jan 2006.

[11] T. Mizunami, T. Djambova, T. Niiho, and S. Gupta, "Bragg gratings in multimode and few-mode optical fibers," *Journal of Lightwave Technology*, vol. 18, no. 2, pp. 230–235, feb 2000.

[12] Y.-G. Nan, I. Chapalo, K. Chah, X. Hu, and P. Mégret, "Through over-clad inscription of FBG in CYTOP optical fiber using phase mask technique and 400 nm femtosecond pulsed laser," *Journal of Lightwave Technology*, vol. 40, no. 9, pp. 3031–3037, may 2022.

[13] A. Ghatak and K. Thyagarajan, "Propagation characteristics of graded index fibers," in *Introduction to fiber optics*. Cambridge University Press, 1998, pp. 173–195.

[14] J. Senior, "Optical fiber waveguides," in *Optical Fiber Communications: Principles and Practice (3rd Edition)*. Pearson Education Limited, 2009, pp. 12–82.

[15] A. W. Snyder and J. D. Love, "Weakly guiding waveguides," in *Optical Waveguide Theory*. LONDON NEW YORK, 1983, pp. 280–300.

[28] H. Kogelnik, "Theory of optical waveguides," in *Guided-Wave Optoelectronics*. Springer Berlin Heidelberg, 1988, pp. 7–88.

[16] F. Mitschke, "Treatment with wave optics," in *Fiber Optics*. Springer, 2016, pp. 29–50.

[17] Corning, *Corning 50/125 Optical Fiber Production Information*. [Online]. Available: http://www.pierluigidamico.it/FO%2050%20125.pdf

[18] R. Olshansky, "Mode coupling effects in graded-index optical fibers," *Applied Optics*, vol. 14, no. 4, p. 935, apr 1975.

[19] A. Hallam, "Mode control in multimode optical fibre and its applications," Ph.D. dissertation, Aston University, 2007.

[20] A. Ghatak and K. Thyagarajan, *I Graded Index Optical Waveguides: A Review*. Elsevier, 1980.

[21] C. Someda and M. Zcboli, "Cutoff wavelengths of guided modes in optical fibres with square-law core profile," *Electronics Letters*, vol. 11, no. 24, p. 602, 1975.

[22] K. Okamoto and T. Okoshi, "Analysis of wave propagation in optical fibers having core with alpha-power refractive-index distribution and uniform cladding," *IEEE Transactions on Microwave Theory and Techniques*, vol. 24, no. 7, pp. 416–421, jul 1976.

[23] T. I. Lukowski and F. P. Kapron, "Parabolic fiber cutoffs: A comparison of theories," *Journal of the Optical Society of America*, vol. 67, no. 9, p. 1185, sep 1977.

[24] E. Bianciardi and V. Rizzoli, "Propagation in graded-core fibres: a unified numerical description," *Optical and Quantum Electronics*, vol. 9, no. 2, pp. 121–133, mar 1977.

[25] K. Kitayama, S. Seikai, and N. Uchida, "Impulse response prediction based on experimental mode coupling coefficient in a 10-km long graded-index fiber," *IEEE Journal of Quantum Electronics*, vol. 16, no. 3, pp. 356–362, mar 1980.

[26] S. P. Ugale and V. Mishra, "Optimization of fiber Bragg grating length for maximum reflectivity," in *2011 International Conference on Communications and Signal Processing*. IEEE, feb 2011, pp. 28–32.

[27] B. E. Pelleg and A. K. Fontecchio, "Modeling light propagation through Bragg reflection gratings with an AdaptedMonte carlo method," *Journal of Lightwave Technology*, vol. 32, no. 12, pp. 2228–2232, jun 2014.

[29] R. Kashyap, "Theory of fiber Bragg gratings," in *Fiber Bragg Gratings*. Elsevier, 2010, pp. 119–189.

[30] P. Lemaire, R. Atkins, V. Mizrahi, and W. Reed, "High pressure H_2 loading as a technique for achieving ultrahigh UV photosensitivity and thermal sensitivity in GeO_2 doped optical fibres," *Electronics Letters*, vol. 29, no. 13, p. 1191, 1993.

[31] The information of the QA6370. [Online]. Available: https://cdn.tmi.yokogawa.com/1/5720/files/IM735371-01E.pdf

© 2022 IEEE. Personal use is permitted, but republication/redistribution requires IEEE permission. See https://www.ieee.org/publications/rights/index.html for more information.